Bromination of Double-Walled Carbon Nanotubes

L. G. Bulusheva,*[,†] A. V. Okotrub,[†] E. Flahaut,[‡,§] I. P. Asanov,[†] P. N. Gevko,[†] V. O. Koroteev,[†] Yu. V. Fedoseeva,[†] A. Yaya,[∥,⊥] and C. P. Ewels*[,∥]

[†]Nikolaev Institute of Inorganic Chemistry SB RAS, 3 Academician Lavrentiev Avenue, Novosibirsk 630090, Russian Federation

[‡]Université de Toulouse; UPS, INP; Institut Carnot Cirimat; 118, route de Narbonne, F-31062 Toulouse cedex 9, France

[§]CNRS, Institut Carnot Cirimat, F-31062 Toulouse, France

[∥]Institut des Materiaux Jean Rouxel, CNRS-Université de Nantes, France

[⊥]Department of Materials Science and Engineering, University of Ghana, Legon, Ghana

ABSTRACT: Double-walled carbon nanotubes (DWCNTs) synthesized by catalytic chemical vapor deposition (CCVD) have been functionalized by bromine vapor at room temperature. At least two different bromine species were detected in the product using X-ray photoelectron spectroscopy (XPS) and thermal gravimetric analysis. The primary form is negatively charged Br_2 molecules exhibiting an intense resonance at ~238 cm^{-1} in the Raman spectrum. The electron transfer from the nanotubes to the adsorbed molecules is detected from C 1s XPS and near-edge X-ray absorption fine structure spectra. The optical absorption spectra reveal that although the metallic nanotubes are more reactive to Br_2, the outer semiconducting nanotubes also readily interact with Br_2 adsorbates. The secondary bromine form is attributed to covalent C−Br bonding, and its possible sources are discussed in the light of quantum-chemical calculations. Analysis of the XPS, Raman, and optical absorption spectra of the Br-DWCNTs annealed at 100−170 °C indicates preservation of a part of bromine molecules in samples that affects the electronic and vibration properties of nanotubes.

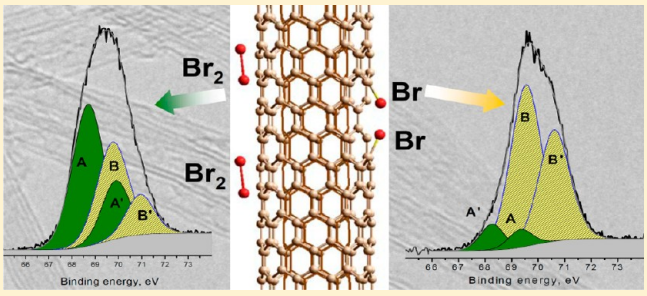

KEYWORDS: *double-walled carbon nanotubes, bromination, charge transfer, X-ray spectroscopy, electronic structure*

INTRODUCTION

Double-walled carbon nanotubes (DWCNTs) composed of two concentric cylinders of graphene are intermediate between single-walled and multiwalled carbon nanotubes (CNTs).[1] As the simplest form of multiwalled CNTs, DWCNTs can be used as a model for better understanding the interactions in multiwalled structures.[2] As compared to single-walled CNT, the double-walled structure allows selective functionalization of the outer wall while protecting the inner tube.[3] Chemical modification is a way to change the properties of CNTs, notably to improve nanotube solubility, bonding with a composite matrix, facilitate charge doping, etc. The interaction of DWCNTs with halogens is one of the most widely studied functionalization routes. It was shown that fluorine atoms are covalently attached to the outer surface of DWCNT,[4,5] and the amount of fluorine and the fluorine distribution are dependent on the fluorination technique used.[6] Raman spectroscopy of iodine-intercalated DWCNTs revealed charge transfer between the outer tubes and adsorbed poly iodide anions.[7]

In terms of reactivity, bromine is intermediate between fluorine and iodine. Bromine has been shown to form molecular complexes[8] as well as covalent bonding[9] with a DWCNT surface. The character of interaction between DWCNTs and gaseous Br_2 has been revealed from an analysis of Raman spectra recorded at different excitation energies.[8,10,11] The Br−Br stretching mode is downshifted compared with solid bromine, indicative of charge transfer from a nanotube to an adsorbate. Metallic nanotubes (even if they constitute the inner tubes) are especially sensitive to the presence of Br_2 molecules. DWCNT bromination has been achieved under microwave-assisted (MiW) conditions, and covalent attachment of bromine atoms to the nanotube surface was detected from the energy position of the peaks in the Br 3d and Br 3p core level spectra.[9] Bromine, covalently attached to the graphitic surface, can be used to couple organic residuals via chemical substitution reactions. It has been shown that plasma-brominated graphitic materials readily interact with amines and water through a conversion of the C−Br groups to $-NH_2$, alkyl$-NH_2$, and −OH functionalities.[12] Compared to fluorination the concentration of attached bromine atoms is considerably less, thus preserving the majority of the graphitic network intact in subsequent reactions.

Examination of reactivity of carbon pitch and graphite nanoplatelets toward Br_2 vapor has showed a possibility to introduce both ionic and covalent bonds in a material.[13,14] Hence, the ratio of different bromine species should depend

not only on the synthesis conditions (temperature, duration) but on the structure of the pristine material as well. The previous identification of solely adsorbed Br_2 molecules in DWCNT samples after exposure to Br_2 vapor can be explained by lack of defects in the CNT shells or by concentration on the one method, namely Raman spectroscopy, for the investigation.[8,10,11,15]

Here we apply of a wide set of experimental techniques to study DWCNTs after reaction with Br_2 vapor at room temperature. The results obtained demonstrate for the first time that both molecular and covalently linked bromine species can be developed simultaneously on the CNT surface. Quantum-chemical modeling suggests that C−Br bonds may be formed at pre-existing defect sites in the walls of CNTs, produced by catalytic chemical vapor deposition (CCVD).

METHODS

Materials. DWCNTs were produced by catalytic decomposition of CH_4 vapor (CCVD, catalytic chemical vapor deposition method) over $Mg_{1-x}Co_xO$ solid solution containing small additions of molybdenum.[16] High-resolution transmission electron microscopy showed that a typical sample consists of ca. 80% DWCNTs, 15% SWCNTs, and a small amount of triple-walled nanotubes. The diameter distribution of the DWCNTs ranged from 0.5 to 2.5 nm for the inner tubes and from 1.2 to 3.2 nm for the outer tubes. DWCNTs were purified by a procedure described elsewhere.[17] Briefly, the sample was heated in air at 450 °C for 1 h followed by treatment with concentrated HCl (37%) in order to dissolve metal oxides formed during the oxidation process and then washed with deionized water and dried at 30 °C in vacuum.

Bromination of DWCNT samples was carried out with Br_2 vapor at room temperature. A sample placed in a Teflon flask was held in a vapor over liquid Br_2 for 7 days. The flask content was then dried by a flow of N_2 up to the termination of Br_2 evolution.

Instrumentation. The structure of the samples was examined by transmission electron microscopy (TEM) on a Jeol 2010 microscope, Raman spectroscopy on a Triplemate spectrometer with an Ar^+ laser (λ = 488 nm), and optical absorption spectroscopy on a Shimadzu UV 3101 PC spectrometer in a wavelength range of 190−3200 nm with 3-nm-resolution. A TEM specimen was prepared on a colloidal carbon substrate via sonication of a nanotube-containing powder suspended in ethanol. To measure optical absorbance, a specimen of pristine DWCNTs or brominated DWCNTs was ultrasonicated in heptane during 1 h and then deposited on a sapphire substrate airbrushing the suspension. The thickness and uniformity of the covering was controlled visually. After the measurement, the sapphire substrate with the brominated sample was annealed in an inert atmosphere at 100 °C for half an hour, and the spectra measurements were repeated. Then the sample was annealed at 400 °C. For statistics, the spectra were recorded in five points of a sample and averaged. Baseline correction was done by a polynomial fit.

Thermogravimetric analysis (TGA) was performed with a SETARAM TAG24 thermobalance. The sample was continuously heated in an argon atmosphere from 20 to 600 °C at a rate of 1 °C/min.

X-ray photoelectron spectroscopy (XPS) study of the initial and brominated DWCNT samples was performed on a SpecsLab PHOIBOS 150 spectrometer using monochromatic Al Kα-radiation (1486.6 eV). To examine the effect of heating on the chemical state of bromine, the brominated sample was resistively heated in a stainless steel holder in the preparation chamber of the spectrometer at 170 °C for 15 min in vacuum (10^{-7} mbar) and cooled to room temperature, and its XPS spectrum was recorded again. The base pressure in the spectrometer chamber during experiments was 10^{-9} mbar. The near-edge X-ray absorption fine structure (NEXAFS) spectra were acquired in the total-electron yield mode at the Berliner Elektronenspeicherring für Synchrotronstrahlung (BESSY) using radiation from the Russian-German beamline. The spectra were normalized to the primary photon current from a gold-covered grid recorded simultaneously. The monochromatization of the incident radiation for the carbon region was ~80 meV full width at half-maximum (fwhm).

Computational Details. Theoretical modeling was carried out using a hybrid method MPW1K[18] within the quantum-chemical program package Jaguar.[19] In the MPW1K method, the exchange functional is a sum of 25% exact Hartree−Fock exchange and 75% Slater local functional[20] including Perdew−Wang 1991[21] gradient correction functional modified by Adamo and Barone,[22] while the correlation is presented by Perdew−Wang 1991 GGA-II local and nonlocal functionals.[21] Atomic orbitals were described by a STO-3G basis set, which was chosen as the optimal basis set describing correctly the Br−Br interactions with a minimum consumption of computational time. The Br_2 molecule bond length relaxed at the MPW1K/STO-3G level is 2.301 Å, exceeding the experimental value of 2.283 Å by less than 1%. An armchair (6,6) tube having 5 hexagons in length and closed by hemispheres was used as a model of a CNT. The geometry of the model with the Br_2 molecule located at different positions over the central part of the cluster was optimized by an analytical gradient method until the energy was converged to better than 5×10^{-5} Hartree/Bohr. Energy of formation of brominated CNTs was calculated as follows: $E^{form} = E^{tot}(model) - E^{tot}(CNT) - E^{tot}(Br_2)$, where E^x is a total energy of the model, the isolated initial CNT cluster, and the free Br_2 molecule, respectively.

RESULTS AND DISCUSSION

TEM images of pristine DWCNT samples and after exposure to Br_2 vapor are shown in Figure 1. The nanotubes are mainly

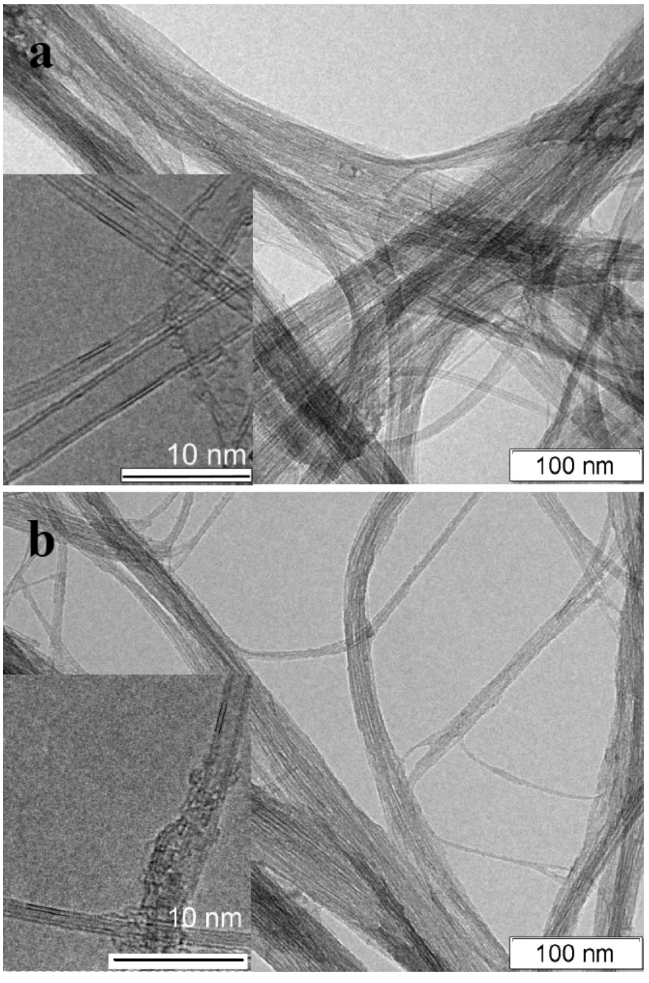

Figure 1. TEM image of pristine DWCNT sample (a) and brominated DWCNT sample (b). The inserts show the individual DWCNTs occurred in the samples.

gathered into the ropes and only in rare cases are in individualized form. From comparison of the images it seems that after bromination the average diameter of DWCNT ropes is slightly reduced and more separated nanotubes are visible. The high-resolution TEM images (inserts in Figure 1) indicate no obvious changes in the morphology of DWCNTs with bromination and notably no detectable increase in the interlayer separation, which would be expected if Br_2 molecules are intercalating between the inner and outer tubes.

The overall XPS spectrum of the brominated DWCNT sample showed signals of carbon, oxygen, and bromine. The bromine concentration estimated from the ratio of the areas of the Br 3d and C 1s lines is ~5.6 at% giving an average stoichiometry of $C_{17}Br$. This is higher than a previous study ($C_{21}Br$) using a similar approach for only 5 days.[8] TGA measurements were used to evaluate the change in the thermal behavior of DWCNTs after bromination (Figure 2). The

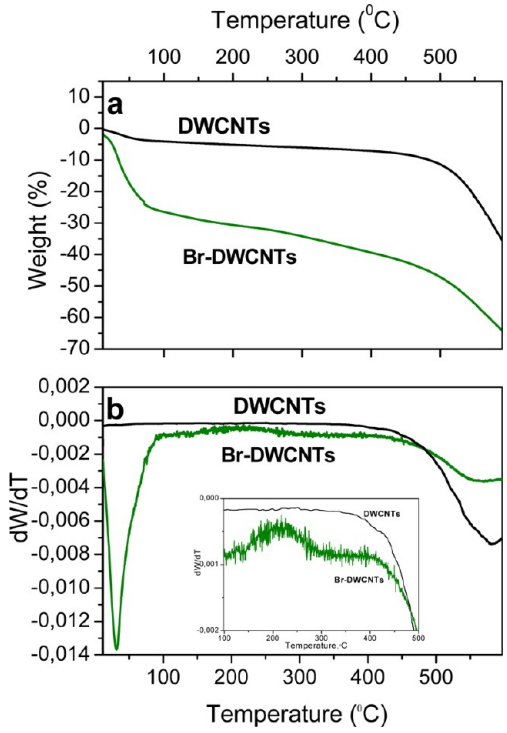

Figure 2. (a) Thermal gravimetric (TG) and (b) differential TG (DTG) curves for pristine and brominated DWCNTs. The insert shows the thermal behavior of the samples in the interval from 100 to 500 °C.

differential TG (DTG) curves show that the weight loss of pristine DWCNTs starts from *ca.* 450 °C, and the sample then loses weight continuously with increasing temperature (Figure 2b). As DWCNTs should not decompose in an inert atmosphere at this temperature[23] we attribute this behavior to a small leak and/or a few impurities in the argon, which could be detectable in DTG given the small quantity of measured specimen. In contrast the weight of the brominated sample strongly drops in a narrow interval from 25 to 75 °C and then slowly decreases until the temperature of DWCNT decomposition (Figure 2a). The total weight loss of the Br–DWCNT sample between 25 and 450 °C is ~38 wt %, corresponding to a bromine content of ~8.4 at%. This value is larger than the total bromine concentration derived from the XPS data. The observed discrepancy is due to surface-sensitivity of XPS and neglect of the oxygen-containing species, which also contribute to the sample loss. A minimum in the DTG curve at 32 °C corresponds to removal of Br_2 molecules that finishes at *ca.* 90 °C (Figure 2b). The sample loses more weight from *ca.* 100 to 190 °C and from *ca.* 240 to 390 °C (the enlarged picture is presented in the insert in Figure 2b). The lower temperature interval can be related to water desorption and decomposition of carboxyl groups.[24] This is consistent with the XPS which shows an increase in the sample oxygen content after bromination from ~2.0 to ~4.6 at%. The sample decomposition with further heating could be consistent with the breaking of covalent C–Br bonds. The main weight loss of the Br–DWCNT sample in this process is observed at *ca.* 310 °C, very close to the temperature of decomposition of DWCNTs (304 °C) brominated under MiW conditions.[9] Note that in our case the peak attributed to the C–Br bonds is broad, contrary to the sharp peak observed in the DTG curve of the MiW-brominated DWCNTs. The peak sharpness indicates the similarity of the C–Br species developed on the nanotube surface after MiW irradiation of aqueous Br_2. Irradiation probably generates bromine radicals interacting with the graphitic network. Dissociation of Br_2 molecules at room temperature, as we show below using quantum-chemical calculations, requires special conditions such as edge carbon atoms. The C–Br bonds formed at various sites of a CNT surface should have different energies which can explain the bromine detachment in an interval from *ca.* 240 to 390 °C.

The effect of bromination on the electronic structure of DWCNTs was checked by comparing the XPS C 1s spectra of the samples before and after the treatment. The spectrum of the initial DWCNTs has a single maximum at 284.5 eV with a shape characteristic of graphitic carbon,[25] which shifts downward to 284.1 eV following bromination (Figure 3a). In the rigid band model, the lowering of the C 1s electron binding energy corresponds to a downshift of the Fermi level, and a similar effect has been observed previously for single-walled CNTs chemically modified by $SOCl_2$.[26] Previous quantum-chemical calculations showed that high bromine concentrations intercalated into a (6,6) metallic armchair CNT crystal dropped the Fermi level by about 0.6 eV.[27] Adsorption of Br_2 molecules on the surface of semiconducting CNTs induces a band corresponding to the electronic states of bromine above the valence edge of the nanotube.[27,28] Parallel orientation of Br_2 molecules on brominated graphene with a $C_{16}Br$ stoichiometry pins the Fermi level ~0.2 eV lower than in pristine graphene.[29] Hence, the shifting of the C 1s peak for the Br–DWCNT sample is attributed to Fermi level lowering due to p-type doping of nanotubes. Attenuation of a feature around 291 eV corresponding to the $\pi \rightarrow \pi^*$ shakeup transition can be ascribed to partial disruption of the π electron system.[30]

The bromine species present on the surface of the DWCNTs was determined from the XPS Br 3d spectra measured for the brominated sample before and after heating. The spectra were fitted by two $3d_{5/2}$–$3d_{3/2}$ spin–orbit doublets (Figure 3b). The components labeled A and B correspond to the Br $3d_{5/2}$ lines, while the higher energy components (A′ and B′) are the Br $3d_{3/2}$ lines. The ratio of the integrated intensities A/A′ as well as the integrated intensities B/B′ is equal to 3/2. The primary contribution to the as-brominated spectrum comes from the first doublet presented by the components A and A′ located at ~68.7 and ~69.9 eV (curve 1 in Figure 3(b)). The components B and B′ of the second doublet have energies ~69.8 and 70.9 eV. Previous XPS studies of brominated carbon black detected

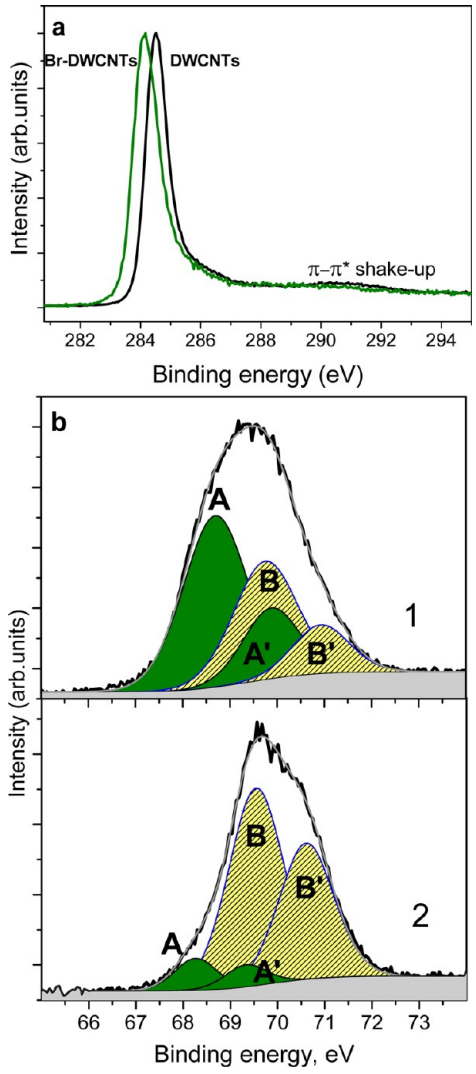

Figure 3. (a) Comparison of XPS C 1s spectra for pristine and brominated DWCNTs. (b) XPS Br 3d spectrum of brominated DWCNTs (1) and that after sample heating at 170 °C (2). The spectra were fitted to two doublets A/A′ and B/B′. The components A and B correspond to the Br $3d_{5/2}$ lines; the components A′ and B′ correspond to the Br $3d_{3/2}$ lines.

different types of bromine bonds depending on the bromination method.[31] A Br $3d_{5/2}$ component with binding energy of 70.0 ± 0.2 eV was assigned to bromine covalently bonded to sp^2 and sp^3 carbon atoms, and in our case these bromine species could be responsible for the appearance of peak B. The lower energy components around 68.5 ± 0.2 and 67.4 ± 0.2 eV were assumed to come from negatively charged bromine derivatives, for example, physically adsorbed BrH, and charge-transfer carbon–Br_2 complexes.[31] Note that the position of the intense component A in the spectrum of Br–DWCNTs is more than 1 eV higher in energy than that assigned to the bromine molecules adsorbed on the carbon black.

To more clearly elucidate the origin of the Br 3d components we measured the XPS spectrum of the Br–DWCNT sample *in situ* heated at 170 °C for 15 min. According to the TGA data any Br_2 molecules should be desorbed in these conditions. With heat treatment, the intensity of the A/A′ doublet is strongly suppressed (curve 2 in Figure 3b). Hence we are able to clearly assign the lower energy Br 3d components A and A′ to the molecular complexes of bromine with DWCNTs. The B/B′ doublet in the spectrum of the heated sample becomes dominant, indicating a more stable structure and/or stronger interaction between carbon and bromine than occurs in charge-transfer complexes. Surprisingly both doublets are shifted toward lower energies compared to the nonheated sample (68.3 and 69.6 eV for the A and B components respectively). It is possible that the remaining nondesorbed bromine molecules are intercalated in DWCNT ropes, and being surrounding by nanotubes they have a larger negative charge than those on the rope surface. Alternatively, the A/A′ doublet located at 68.3/69.3 eV in the heated sample could be assigned to the poly bromine species, for example Br_3^-. The change in the binding energy of the covalently bonded bromine atoms indicates their rearrangement on the CNT surface with the heat treatment. To the best of our knowledge, this is the first reported *in situ* XPS examination of thermal behavior of bromine on the CNT surface.

Assigning the low-energy Br 3d doublet (A/A′) to the Br_2 molecules and the high-energy doublet (B/B′) to the C–Br bonds, we can now estimate the concentration of these bromine species in the gas-phase brominated DWCNTs. The ratio between integrated intensities of the first and second doublet is about 1.7. From a total bromine concentration (~5.6 at%) this ratio yields ~3.5 at% of adsorbed Br_2 and ~2.1 at% of covalently bonded bromine. Although the obtained values are smaller than those calculated from the TGA data, the relative concentration of the two different bromine species has the same value independent of whether XPS or TGA was used for the estimation.

NEXAFS spectra measured near the CK-edge of pristine and brominated DWCNTs show two main resonances at 285.4 and 291.7 eV corresponding to 1s→π^* and 1s→σ^* transitions (Figure 4). The spectrum of the Br–DWCNT sample exhibited

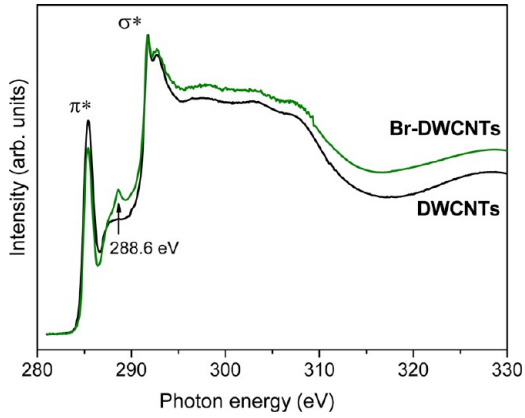

Figure 4. NEXAFS spectra measured near the CK–edge of pristine and brominated DWCNTs, normalized on the σ^* resonance intensity. The arrow shows a new resonance in the brominated sample.

a lowering of π^* resonance and appearance of new peak at 288.6 eV. The CK-edge spectrum of CCVD single-walled CNTs immersed in Br_2 liquid for 2 days also showed a pronounced feature at 288.6 eV assigned to bonds between the CNT sidewalls and bromine atoms.[32] However we note that other peak assignments lie in the same energy range, for example the 1s→π^* (C═O) transitions within carboxyl groups occur at close energy.[33] The decrease of the π^* resonance in the spectrum of the Br–DWCNTs is caused by depletion of

the π states, which is due to covalent linking of carbon atoms with bromine and transferring of electron density to the adsorbed Br_2 molecules.

The Raman spectrum of pristine DWCNTs shows two groups of frequencies in the radial breathing mode (RBM) range (Figure 5a). The peaks between 250 and 350 cm^{-1}

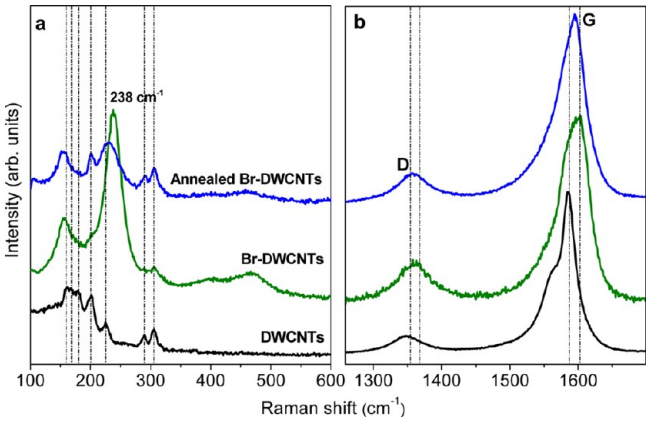

Figure 5. Raman spectra taken with 488 nm for pristine DWCNTs, brominated DWCNTs, and those annealed in a vacuum at 170 °C for 15 min: (a) radial breathing mode spectral region and (b) tangential mode spectral region.

correspond to the inner tubes, while the lower frequency peaks are related to the outer tubes. According to the Kataura plot for the electronic transition energies,[34] at the 488-nm excitation metallic inner CNTs and semiconducting outer CNTs are in resonance. In contrast, the spectrum of the Br–DWCNT sample is dominated by a strong peak at 238 cm^{-1} assigned to the Br–Br stretching band of the Br_2 molecule,[8] with a broad overtone around 473 cm^{-1}. The Br_2 vibration is highly downshifted compared with gaseous Br_2 (324 cm^{-1})[35] indicating negative charging of the adsorbed molecules and is very close to that observed previously in bromine intercalated graphite (~242 cm^{-1}).[36]

Comparison of the Raman spectra of different carbon materials showed that the bromine vibrational frequency is very dependent on the type of carbon surface used for the adsorption or intercalation of the Br_2 molecules.[11] The large width and intensity of the peak at 238 cm^{-1} (Figure 5a) makes precise measurement of the position and intensity of the RBM peaks difficult. It seems that upon bromination the peaks associated with the inner nanotubes are only slightly upshifted (no more than 2 cm^{-1}) and significantly drop in intensity due to the charge doping. In the low-frequency range, the sample exhibits an intense peak at 156 cm^{-1} not observed for the pristine sample.

The Raman spectra of the initial and brominated samples in the 1200–1700 cm^{-1} range were normalized on the intensity of the G band (Figure 5b). The increase in the D band intensity with bromination indicates defect formation in the DWCNT walls. These could be attributed to nanotube surface functionalization with bromine and oxygen-containing groups in agreement with the XPS data. Moreover, the adsorbed Br_2 molecules will locally deform the nanotube structure thus enhancing the D band intensity. In addition after bromination we observe an upshift of the Raman scattering for the D band by ~14 cm^{-1} and for the G band by ~16 cm^{-1}, attributed to DWCNT doping.[37] The G band broadening is caused by different frequency shifts for the semiconducting outer nanotube and metallic inner nanotubes with charge transfer to the adsorbed Br_2 molecules.[8]

Raman scattering measurements on the Br–DWCNTs annealed in a vacuum chamber of X-ray spectrometer (170 °C for 15 min) confirmed retention of a portion of Br_2 molecules in the sample, which have been detected in XPS. The peak located around 230 cm^{-1} (Figure 5a) is likely to be a superposition of the Br–Br stretching mode and the RBM peak existing in the Raman spectrum of the pristine DWCNTs at 226 cm^{-1}. Debromination results in complete recovery of the peaks corresponding to the inner nanotubes. This result shows that the amount of transferred charge from the inner nanotubes depends on the concentration of Br_2 molecules. Note that the peak at 156 cm^{-1} developed during DWCNT bromination still has high intensity in the spectrum of the annealed sample, masking the RBM peaks of the outer nanotubes. Hence, we attribute this peak to charged bromine species, probably to polyanions.

After partial removal of Br_2 from the sample, the intensity of the D band markedly decreases while remaining higher than in the initial DWCNT sample (Figure 5b). Taking into account the TGA and XPS data we conclude that among sp^3 carbon atoms linked with bromine and oxygen-containing groups, adsorbed Br_2 molecules also contribute to the enhancement of the D band due to breaking of the nanotube symmetry. The position of the G band in the spectrum of the annealed Br–DWCNTs is intermediate relative to those for the initial and brominated samples.

Optical absorption spectroscopy gives information for all nanotubes present in a sample. The spectra of DWCNTs before and after bromination and the spectra of Br–DWCNTs annealed at 100 and 400 °C correspond to the removal of Br_2 and destruction of C–Br bonds (see Figure 6). It is well-known

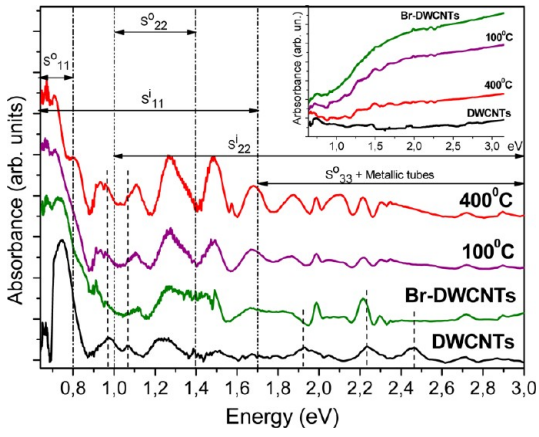

Figure 6. Optical absorption spectra for pristine and brominated DWCNTs and the brominated samples annealed in vacuum at 100 and 400 °C background corrected and scaled for better visibility. The insert shows the spectra without background correction. Dashed lines indicate peaks whose intensity or position was strongly modified by bromination.

that the CNT samples show broad absorption background induced by plasmon resonances in carbon species, nanotube aggregation and chemical functionalization, congestion from closely spaced peaks, etc.[38] Bromination of DWCNTs adds a spectral background that increases toward higher energy (insert in Figure 6). This contribution is gradually reduced with the

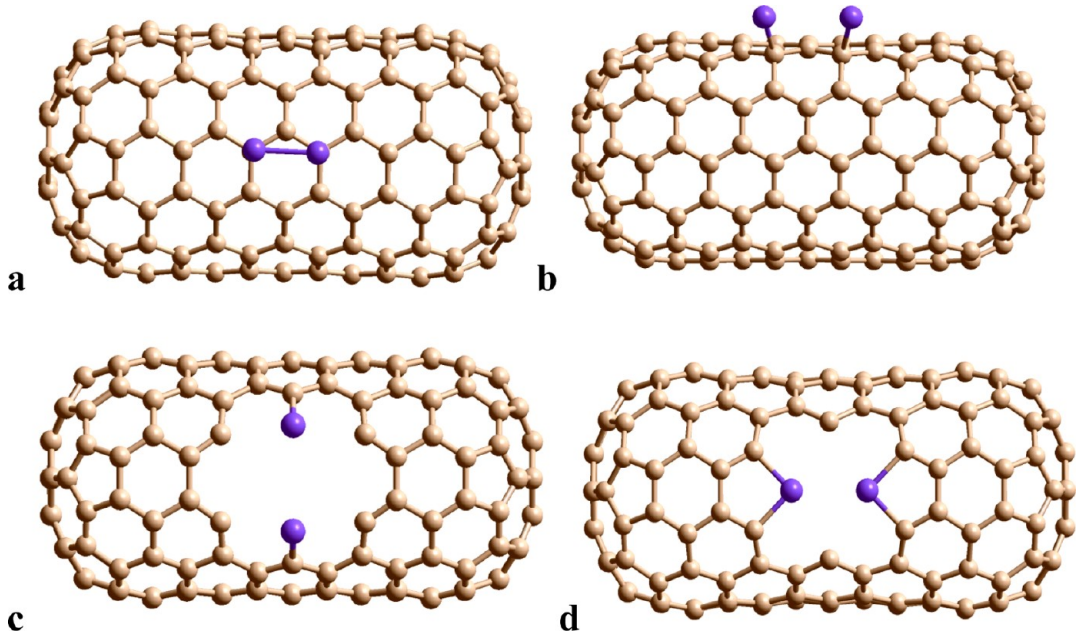

Figure 7. Carbon nanotube with Br_2 molecule adsorbed over carbon atoms *meta*-located in hexagon (a), and covalent bonding of bromine with nanotube surface (b), edge atoms of a hexagonal vacancy in a nanotube wall in *para*-position (c), and forming pentagonal C_4Br rings (d). The bromine atoms are highlighted in purple.

annealing of the brominated sample. To more clearly resolve the absorption peaks from interband electronic transitions, the as-measured curves were corrected by subtracting background and normalized on the maximal intensity. The optical absorption spectrum of the pristine DWCNTs is weakly resolved (Figure 6) because nanotubes are bundled.[39] The improved resolution after bromination is due to an increased intertube distance as a result of intercalation. A similar effect has been observed in the optical absorption spectra of fluorinated DWCNTs.[40] A previous study of pristine DWCNTs using Raman, optical absorption, and photoluminescence spectroscopy revealed that mainly semiconducting outer nanotubes (S^o) and inner nanotubes (S^i) are seen in the low-energy region up to 1.7 eV, while the interband electronic transitions of metallic nanotubes appear at higher energies.[41] Based on this, our optical absorbance peaks are assigned schematically to specific transitions in Figure 6.

The decrease in the relative intensity of peaks at 0.95 and 1.07 eV (dashed lines in Figure 6) after bromination indicates bromine interaction with 1.7−1.8 nm diameter semiconducting nanotubes.[42] These can either be the outer wall of a DWCNT or single-walled CNTs. A recent study of Br_2 interaction with single-walled CNTs revealed a stronger charge-transfer for metallic versus semiconducting CNTs, leading to the suggestion of a separation treatment dependent on conductivity behavior.[43] Our results show that the outer semiconducting nanotubes of DWCNTs also readily interact with bromine. The well-distinguished peaks at 1.92 and 2.24 eV (dashed lines in Figure 6) come from metallic (9,9) and (9,6) nanotubes.[44] The red shift of these peaks after bromination is likely due to charge transfer from the inner nanotubes to the outer nanotubes covered by Br_2 molecules. A sharp peak at 1.99 eV exhibited in the spectrum of Br-DWCNTs corresponds to the second transition energy of semiconducting (10,3) nanotube.[40] Finally we should mention complete disappearance of the peak at 2.46 eV from the metallic (10,1) nanotube after bromination. The spectral changes at energies higher than ∼1.4 eV are related with single-walled CNTs and the inner shells of DWCNTs. Although the inner shells are protected by the outer tubes, they are apparently nevertheless perturbed by doping and resulting charge transfer.

Annealing of the brominated sample at 100 °C increases relative intensity of the peaks within the 0.9−1.9 eV spectral region due to debromination of the outer tubes. Additional intensity increase observed in the spectrum of the Br-DWCNTs annealed at 400 °C shows that not all Br_2 molecules were removed from the sample after the treatment at 100 °C, and this result agrees with the XPS data. However debromination does not recover the pristine optical absorption spectrum. As compared to the spectrum of initial DWCNTs the spectrum of the debrominated sample shows increases in the peak-to-valley ratio that reflects a decrease in aggregation of nanotubes[38] in agreement with the TEM analysis.

We next try to explain the bromination process. The results thus far suggest at least two types of bromine interaction with DWCNTs, as seen for example in the TGA with more than one weight loss peak associated with bromine and the dual set of XPS peaks. We can use quantum chemical calculations to eliminate some possible models. The predominant species is likely to be molecule Br_2, as shown previously in the literature for CNTs, graphene, and graphite.[8,10,11,29] In our calculations, the most energy stable Br_2−CNT complex is formed with a Br_2 molecule over *meta*-sites of a carbon hexagon (Figure 7a, Table 1). This complex is stabilized by the close match between the Br−Br length (2.302 Å) and the C−C distance of 2.497 Å that allows interaction of both bromine atoms with the carbon atoms. A similar Br_2 position on the surface of zigzag CNTs was obtained using DFT calculations within the local density approximation,[28] while perpendicular Br_2 molecular adsorption was found to be preferable on graphene.[29,45] It is likely that the precise orientation of Br_2 molecules will be dependent on the curvature of graphene sheet as well as stoichoimetry of the brominated sample.[46] The change in the binding energy for the

Table 1. Energetic and Structural Data Obtained from the Brominated CNT Models at the MPW1K/STO-3G Calculation Level[b]

bonding species	E^{form}	d_{C-Br}	Br 3d (relative value)[a]
Br_2−CNT	0.22	3.110	50.76 (0)
Br−C(*surface*)	2.95	2.038	48.37 (−2.39)
Br−C(*edge*)	−8.19	1.877	51.86 (+1.10)
C−Br−C	−10.21	1.936	55.57 (+4.81)

[a]The value in parentheses is the shift relative to the eigenvalue of Br 3d levels in the Br_2 molecule adsorbed on the CNT surface. [b]Energy of formation (eV), minimal C−Br distance (Å), average eigenvalue of the Br 3d levels (eV). Bonding species denoted Br_2−CNT, Br−C(*surface*), Br−C(*edge*), and C−Br−C correspond to the models shown in Figure 7 (a, b, c, and d).

possible Br_2-graphene configurations is within 0.15 eV,[29] thus the rotation barrier of the molecule should be small.

One possibility for the secondary species is dissociated Br_2 forming direct C−Br bonds with the nanotube surface. We therefore modeled a (6,6) nanotube, placing Br_2 either above neighboring carbon hexagon sites or dissociated on *meta*-sites of a carbon hexagon (Figure 7b). The calculations show that although the dissociated structure is metastable, it is around 2.7 eV less stable than the molecular form (Table 1), eliminating spontaneous Br_2 surface dissociation as a possible candidate. Another possible candidate is bromination of surface defects. X-ray fluorescent CKα-spectra of graphite and DWCNTs produced in the same CCVD conditions shows enhanced high-energy intensity for the DWCNTs attributed to defects in the tube walls.[5] Calculated CKα-spectra for CNTs with various defects showed an enhancement of density of the weakly bonding states similar to that observed in the experiment occurs for electrons from carbon dangling bonds surrounding a missing hexagon in the graphitic network.[47,48] Other sources of dangling bond states may be unterminated sites at open tube tips, and topological tube wall defects such as dislocations. In our calculations, a Br_2 molecule placed above such a hexavacancy spontaneously dissociates. Depending on the starting position of the molecule, a bromine atom is linked to one carbon atom (Figure 7c) or to two carbon atoms forming a pentagonal C_4Br ring (Figure 7d). The C−Br bonds in both structures are shorter than those of bromine atoms covalently bound to the surface of a perfect (6,6) nanotube (Table 1). As expected the interaction of a Br_2 molecule with under-coordinated carbon atoms in a CNT wall is highly exothermic (Table 1). Although the vacancy has the same number and arrangement of missing carbon atoms in the models presented in Figure 7c, d and both contain two bromine atoms, the electronic and vibrational properties of the brominated CNTs are different.

The XPS Br 3d line (curve 1 in Figure 3b) can be analyzed in light of the calculations. Two components, separated by ~1.18 eV, were obtained by spectral decomposition, the lower binding energy species being attributed to surface absorbed molecular bromine. To compare the calculation results with the experiment we calculated the shift of the Br 3d orbital eigenvalue in the model with covalently bonded bromine relative to that in the Br_2−CNT complex. The obtained values are collected in the Table 1. Bromine covalently bound to the perfect CNT surface is predicted to have a peak in the Br 3d XPS spectrum at a lower energy than that of molecular Br_2, eliminating it as a candidate for the second component. Bromine bound to carbon atom dangling bonds, for example at vacancies or open tube tips, are predicted to have higher binding energy than that of adsorbed Br_2. Indeed the experimental Br 3d level shift matches well the calculated shift of 1.10 eV obtained for the model where bromine atoms are bonded to carbon atoms at the zigzag edge of hexavacancy (Figure 7c). Thus bromine in these sorts of configurations could give rise to the weak secondary peaks seen in XPS. The absence of an XPS component corresponding to bromine in the more stable C−Br−C configuration (Figure 7d) is probably due to a reduction in the ratio of bromine to carbon dangling bonds in the experimental system as compared to the calculations, either due to an increased bromine concentration or partial termination of dangling bonds by oxygen-containing species.

■ CONCLUSION

The interaction of DWCNTs with gaseous Br_2 at room temperature was studied using TGA, Raman, optical absorption, XPS, and NEXAFS spectroscopy coupled with quantum-chemical calculations. Two main bromine species were identified in the brominated sample from the XPS analysis: the primary species adsorbed Br_2 molecules and a lower concentration more stable secondary species, possibly due to covalent attachment of bromine to dangling carbon bonds. The downshift of the Br−Br stretching vibration and depletion of the π^* states in the Br−DWCNTs demonstrate the charge transfer from carbon nanotube to the adsorbed Br_2 molecules. The Raman and optical absorption spectra reveal that although the metallic nanotubes are more reactive to Br_2 (even when they constitute the inner nanotubes), the outer semiconducting nanotubes also readily interact with Br_2 adsorbates. The better resolved optical absorption peaks after bromination-debromination treatment indicates that interaction with Br_2 causes partial debundling of nanotubes, and this procedure could be used for DWCNT dispersion. Quantum-chemical calculations of interaction of bromine with an armchair (6,6) CNT confirm that Br_2 molecules adsorb on the surface of perfect nanotubes, while they can dissociate near dangling bond defect sites with the formation of covalent C−Br bonds. Thus, any covalent attachment of bromine to the graphitic surface achieved at room temperature is likely related with defects in the DWCNTs produced by the CCVD method. Covalently bonded bromine can provide the chemical activity of nanotubes to couple organic residues *via* substitution reactions.

■ AUTHOR INFORMATION

Corresponding Author

*L.G.B.: e-mail bul@niic.nsc.ru. C.P.E.: e-mail chris.ewels@cnrs-imn.fr.

Notes

The authors declare no competing financial interest.

■ ACKNOWLEDGMENTS

We thank Mr. A. V. Ishchenko for the TEM measurements. The work was supported by the bilateral Program "Russian-German Laboratory at BESSY, the French Embassy in Russia, and the COST project MP0901 "NanoTP". C.P.E. acknowledges the NANOSIM-GRAPHENE project no. ANR-09-NANO-016-01 funded by the French National Agency

(ANR) in the frame of its 2009 programme in Nanosciences, Nanotechnologies and Nanosystems (P3N2009).

REFERENCES

(1) Shen, C.; Brozena, A. H.; Wang, Y. H. *Nanoscale* **2011**, *3*, 503.
(2) Dresselhaus, M. S. *ACS Nano* **2010**, *4*, 4344.
(3) Brozena, A. H.; Moskowitz, J.; Shao, B.; Deng, S.; Liao, H.; Gaskell, K. J.; Wang, Y. H. *J. Am. Chem. Soc.* **2010**, *132*, 3932.
(4) Muramatsu, H.; Kim, Y. A.; Hayashi, T.; Endo, M.; Yonemoto, A.; Arikai, H.; Okino, F.; Touhara, H. *Chem. Commun.* **2005**, 2002.
(5) Bulusheva, L. G.; Gevko, P. N.; Okotrub, A. V.; Lavskaya, Yu. V.; Yudanov, N. F.; Yudanova, L. I.; Abrosimov, O. G.; Pazhetnov, E. M.; Boronin, A. I.; Flahaut, E. *Chem. Mater.* **2006**, *18*, 4967.
(6) Bulusheva, L. G.; Fedoseeva, Yu. V.; Okotrub, A. V.; Flahaut, E.; Asanov, I. P.; Koroteev, V. O.; Yaya, A.; Ewels, C. P.; Chuvilin, A. L.; Felten, A.; et al. *Chem. Mater.* **2010**, *22*, 4197.
(7) Cambedouzou, J.; Sauvajol, J.-L.; Rahmani, A.; Flahaut, E.; Peigney, A.; Laurent, C. *Phys. Rev. B* **2004**, *69*, 235422.
(8) Souza Filho, A. G.; Endo, M.; Muramatsu, H.; Hayashi, T.; Kim, Y. A.; Barros, E. B.; Akuzawa, N.; Samsonidze, Ge. G.; Saito, R.; Dresselhaus, M. S. *Phys. Rev. B* **2006**, *73*, 235413.
(9) Colomer, J.-F.; Marega, R.; Traboulsi, H.; Meneghetti, M.; Van Tendeloo, G.; Bonifazi, D. *Chem. Mater.* **2009**, *21*, 4747.
(10) do Nascimento, G. M.; Hou, T.; Kim, Y. A.; Muramatsu, H.; Hayashi, T.; Endo, M.; Akuzawa, N.; Dresselhaus, M. S. *J. Phys. Chem. C* **2009**, *113*, 3934.
(11) do Nascimento, G. M.; Hou, T.; Kim, Y. A.; Muramatsu, H.; Hayashi, T.; Endo, M.; Akuzawa, N.; Dresselhaus, M. S. *Nano Lett.* **2009**, *8*, 4168.
(12) Friedrich, J. F.; Wettmarshausen, S.; Hanelt, S.; Mach, R.; Mix, R.; Zeynalov, E. B.; Meyer-Plath, A. *Carbon* **2010**, *48*, 3884.
(13) Klimenko, I. V.; Zhuravleva, T. S.; Geskin, V. M.; Jawhary, T. *Mater. Chem. Phys.* **1998**, *56*, 14.
(14) Li, J.; Vaisman, L.; Marom, G.; Kim, J.-K. *Carbon* **2007**, *45*, 744.
(15) Chen, G.; Bandow, S.; Margine, E. R.; Nisoli, C.; Kolmogorov, A. N.; Crespi, V. H.; Gupta, R.; Sumanasekera, G. U.; Iijima, S.; Eklund, P. C. *Phys. Rev. Lett.* **2003**, *90*, 257403.
(16) Flahaut, E.; Bacsa, R.; Peigney, A.; Laurent, Ch. *Chem. Commun.* **2003**, 1442.
(17) Osswald, S.; Flahaut, E.; Ye, H.; Gogotsi, Y. *Chem. Phys. Lett.* **2005**, *402*, 422.
(18) Lynch, B. J.; Fast, P. L.; Harris, M.; Truhlar, D. G. *J. Phys. Chem. A* **2000**, *104*, 4811.
(19) *Jaguar*, version 6.5; Schrödinger, LLC: New York, NY, 2005.
(20) Slater, J. C. *Quantum Theory of Molecules and Solids, Vol. 4: The Self−Consistent Field for Molecules and Solids*; McGraw-Hill: New York, 1974.
(21) Perdew, J. P.; Chevary, J. A.; Vosko, S. H.; Jackson, K. A.; Pederson, M. R.; Singh, D. J.; Fiolhais, C. *Phys. Rev. B* **1992**, *46*, 6671.
(22) Adamo, C.; Barone, V. *J. Chem. Phys.* **1998**, *108*, 664.
(23) Kim, Y. A.; Muramatsu, H.; Hayashi, T.; Endo, M.; Terrones, M.; Dresselhaus, M. S. *Chem. Phys. Lett.* **2004**, *398*, 87.
(24) Kuznetsov, V. L.; Butenko, Yu. V. In *Ultra Nanocrystalline Diamond*; Shenderova, O. A., Gruen, D. M., Eds.; William Andrew Publishing: Norwich, New York, U.S.A., 2006; p 403.
(25) Estrade-Szwarckopf, H. *Carbon* **2004**, *42*, 1713.
(26) Dettlaff-Weglikowska, U.; Skákalová, V.; Graupner, R.; Jhang, S. H.; Kim, B. H.; Lee, H. J.; Ley, L.; Park, Y. W.; Berber, S.; Tomanek, D.; Roth, S. *J. Am. Chem. Soc.* **2005**, *127*, 5125.
(27) Jhi, S.-H.; Louie, S. G.; Cohen, M. L. *Solid State Commun.* **2002**, *123*, 495.
(28) Park, N.; Miyamoto, Y.; Lee, K.; Choi, W. I.; Ihm, J.; Yu, J.; Han, S. *Chem. Phys. Lett.* **2005**, *403*, 135.
(29) Yaya, A.; Ewels, C. P.; Suarez-Martinez, I.; Wagner, Ph.; Lefrant, S.; Okotrub, A.; Bulusheva, L.; Briddon, P. R. *Phys. Rev. B* **2011**, *83*, 045411.
(30) Wepasnick, K. A.; Smith, B. A.; Schrote, K. E.; Wilson, H. K.; Diegelmann, S. R.; Fairbrother, D. H. *Carbon* **2011**, *49*, 24.
(31) Papirer, E.; Lacroix, R.; Donnet, J.-B.; Nanse, G.; Fioux, P. *Carbon* **1994**, *32*, 1341.
(32) Zhong, J.; Song, L.; Wu, Z.-Y.; Xie, S.-S.; Abbas, M.; Ibrahim, K.; Qian, H. *Carbon* **2006**, *44*, 866.
(33) Kuznetsova, A.; Popova, I.; Yates, J. T., Jr.; Bronikowski, M. J.; Huffman, C. B.; Liu, J.; Smalley, R. E.; Hwu, H. H.; Chen, J. G. *J. Am. Chem. Soc.* **2001**, *123*, 10699.
(34) Jorio, A.; Fantini, C.; Pimenta, M. A.; Capaz, R. B.; Samsonidze, Ge. G.; Dresselhaus, G.; Dresselhaus, M. S.; Jiang, J.; Kobayashi, N.; Grüneis, A.; Saito, R. *Phys. Rev. B* **2005**, *71*, 075401.
(35) Cahill, J. E.; Leroi, G. E. *J. Chem. Phys.* **1969**, *51*, 4514.
(36) Eklund, P. C.; Kambe, N.; Dresselhaus, G.; Dresselhaus, M. S. *Phys. Rev. B* **1978**, *18*, 7069.
(37) do Nascimento, G. M.; Hou, T.; Kim, Y. A.; Muramatsu, H.; Hayashi, T.; Endo, M.; Akuzawa, N.; Dresselhaus, M. S. *Carbon* **2011**, *49*, 3585.
(38) Naumov, A. V.; Ghosh, S.; Tsyboulski, D. A.; Bachilo, S. M.; Weisman, R. B. *ACS Nano* **2011**, *5*, 1639.
(39) Hertel, T.; Hagen, A.; Talalaev, V.; Arnold, K.; Hennrich, F.; Kappes, M.; Rosenthal, S.; McBride, J.; Ulbricht, H.; Flahaut, E. *Nano Lett.* **2005**, *5*, 511.
(40) Gevko, P. N.; Bulusheva, L. G.; Okotrub, A. V.; Yudanov, N. F.; Yushina, I. V.; Grachev, K. A.; Pugachev, A. M.; Surovtsev, N. V.; Flahaut, E. *Fullerenes, Nanotubes, Carbon Nanostruct.* **2006**, *14*, 233.
(41) Iakoubovskii, K.; Minami, N.; Ueno, T.; Kazaoui, S.; Kataura, H. *J. Phys. Chem. C* **2008**, *112*, 11194.
(42) Barone, V.; Peralta, J. E.; Wert, M.; Heyd, J.; Scuseria, G. E. *Nano Lett.* **2005**, *5*, 1621.
(43) Chen, Z.; Du, X.; Du, M.-H.; Rancken, C. D.; Cheng, H.-P.; Rinzler, A. G. *Nano Lett.* **2003**, *3*, 1245.
(44) Barone, V; Peralta, J. E.; Scuseria, G. E. *Nano Lett.* **2005**, *5*, 1830.
(45) Fan, X.; Liu, L.; Kuo, J.-L.; Shen, Z. *J. Phys. Chem. C* **2010**, *114*, 14939.
(46) Widenkvist, E.; Boukhvalov, D. W.; Rubino, S.; Akhtar, S.; Lu, J.; Quinlan, R. A.; Katsnelson, M. I.; Leifer, K.; Grennberg, H.; Jansson, U. *J. Phys. D: Appl. Phys.* **2009**, *42*, 112003.
(47) Bulusheva, L. G.; Okotrub, A. V.; Dettlaff−Weglikowska, U.; Roth, S.; Heggie, M. I. *Carbon* **2004**, *42*, 1095.
(48) Belavin, V. V.; Okotrub, A. V.; Bulusheva, L. G. *Phys. Solid State* **2002**, *44*, 663.